



Zinc mediates the SREBP-SCD axis to regulate lipid metabolism in *Caenorhabditis elegans*^S

Jing-Jing Zhang,^{*,†} Jun-Jun Hao,[§] Yu-Ru Zhang,^{**} Yan-Li Wang,^{*} Ming-Yi Li,[†] Hui-Lai Miao,[†] Xiao-Ju Zou,^{1,††} and Bin Liang^{1,*,†}

Key Laboratory of Animal Models and Human Disease Mechanisms of the Chinese Academy of Sciences and Yunnan Province* and State Key Laboratory of Genetic Resources and Evolutionary and Functional Genomics,[§] Kunming Institute of Zoology, Chinese Academy of Sciences, Kunming 650223, China; Department of Hepatobiliary Surgery,[†] Affiliated Hospital of Guangdong Medical University, Zhanjiang 524001, China; College of Fisheries,^{**} Henan Normal University, Xinxiang, Henan 453007, China; and Department of Life Science and Biotechnology,^{††} Key Laboratory of Special Biological Resource Development and Utilization of University in Yunnan Province, Kunming University, Kunming 650214, China

Abstract Maintenance of lipid homeostasis is crucial for cells in response to lipid requirements or surplus. The SREBP transcription factors play essential roles in regulating lipid metabolism and are associated with many metabolic diseases. However, SREBP regulation of lipid metabolism is still not completely understood. Here, we showed that reduction of SBP-1, the only homolog of SREBPs in *Caenorhabditis elegans*, surprisingly led to a high level of zinc. On the contrary, zinc reduction by mutation of *sur-7*, encoding a member of the cation diffusion facilitator (CDF) family, restored the fat accumulation and fatty acid profile of the *sbp-1* (*ep79*) mutant. Zinc reduction resulted in iron overload, which thereby directly activated the conversion activity of stearyl-CoA desaturase (SCD), a main target of SREBP, to promote lipid biosynthesis and accumulation. However, zinc reduction reversely repressed SBP-1 nuclear translocation and further downregulated the transcription expression of SCD for compensation. Collectively, we revealed zinc-mediated regulation of the SREBP-SCD axis in lipid metabolism, distinct from the negative regulation of SREBP-1 or SREBP-2 by phosphatidylcholine or cholesterol, respectively, thereby providing novel insights into the regulation of lipid homeostasis.—Zhang, J.-J., Hao, Y.-R., Zhang, Y.-L., Wang, M.-Y., Li, H.-L., Miao, X.-J., Zou, and B. Liang. Zinc mediates the SREBP-SCD axis to regulate lipid metabolism in *Caenorhabditis elegans*. *J. Lipid Res.* 2017. 58: 1845–1854.

Supplementary key words sterol regulatory element-binding protein • stearyl-CoA desaturase • lipid homeostasis

This work was supported by Strategic Priority Research Program of the Chinese Academy of Sciences Grant XDB13030600; National Natural Science Foundation of China Grants 31671230, 31600963, 31171134, U1202223, 31401014, and 31460268; Natural Science Foundation of Yunnan Province Grants P0120160119 and 2013FA042; Yunnan Provincial Science and Technology Department Grant 2014HB022; Yunnan Oversea High-level Talents Program Grant 2015HA040; and China Postdoctoral Science Foundation Grant 2017M613018. The authors declare that they have no competing interests.

Manuscript received 25 April 2017 and in revised form 12 July 2017.

Published, JLR Papers in Press, July 14, 2017
DOI <https://doi.org/10.1194/jlr.M077198>

Lipids, including fatty acids, triglycerides, and cholesterol, are important membrane components, signaling molecules, and energy reservoirs. To grow, proliferate, and survive, the cell must evolve certain mechanisms to quickly respond to lipid requirements or surplus. The transcription factors, SREBPs, play essential roles to regulate the biosynthesis of fatty acids, triglycerides, and cholesterol to meet the needs of the cell (1–5). In mammals, SREBPs are encoded by two genes, *SREBF-1* and *SREBF-2*. *SREBF-1* is transcribed by alternative promoter usage into two isoforms, *SREBP-1a* and *SREBP-1c*, of which *SREBP-1c* mainly regulates fatty acid metabolism (2). SREBP-2 regulates the transcriptional expression of genes mostly participating in cholesterol metabolism (1, 2, 6). Reciprocally, SREBP-1 is also negatively regulated by phosphatidylcholine (PC) (7) and cholesterol negatively regulates the processing of SREBP-2 (6).

The expression and activity of SREBPs have been implicated in metabolic syndromes (8). SREBP-1c has been implicated in type 2 diabetes mellitus, insulin resistance in skeletal muscle, and the pathogenesis of β -cell dysfunction (9–11). Hepatic *SREBP-1c* levels are increased in animal models of insulin resistance (12, 13). Sequence variations at the *SREBF1* locus were linked to type 2 diabetes mellitus (14–16) and increased expression levels of SREBPs and genetic polymorphisms have shown associations with CVDs (17, 18). Meanwhile, many rodent models generated by either overexpression or knockout of SREBPs clearly indicate that dysfunction of SREBPs absolutely results in dyslipidemia: aberrant lipid metabolism in the liver, adipose

Abbreviations: BP, 2,2'-dipyridyl; CDF, cation diffusion facilitator; PC, phosphatidylcholine; QPCR, quantitative real-time PCR; RNAi, RNA interference; SCD, stearyl-CoA desaturase; TAG, triacylglycerol; TPEN, *N,N,N',N'*-tetrakis (2-pyridylmethyl) ethylenediamine; WGS, whole genome sequencing.

¹To whom correspondence should be addressed.

e-mail: xiaojuzou@163.com (X.-J.Z.); liangb@mail.kiz.ac.cn (B.L.)

^SThe online version of this article (available at <http://www.jlr.org>) contains a supplement.

tissue, pancreas, and other organs and tissues (19–26). Therefore, the biological functions of SREBPs must be tightly regulated to maintain lipid homeostasis.

In spite of the above established regulatory circuits of SREBP-2 by cholesterol (6), SREBP-1 by PC (7), and *Drosophila* (d)SREBP by phosphatidylethanolamine (27), it is still arguable that other unknown factors may participate in the SREBPs' regulation of lipid metabolism. The activities and functions of SREBPs in lipid metabolism are highly evolutionarily conserved across metazoans. The model organism, *Caenorhabditis elegans*, contains only one SREBP family member encoded by *sbp-1*. Similar to its mammalian homologs, SBP-1 also regulates fatty acid (28–31), PC (7), and cholesterol metabolism (32, 33). Depletion of *sbp-1* by RNA interference (RNAi) knockdown (29, 32, 34) or deletion (28) leads to altered fatty acid profiles and lowered fat stores. Through a forward genetic screen of suppressors of the *sbp-1(ep79)* mutant, we identified that mutations in *sur-7*, encoding a member of the cation diffusion facilitator (CDF) family, could restore the altered lipid profiles of the *sbp-1(ep79)* mutant. Furthermore, we revealed a distinct zinc-mediated SREBP-stearoyl-CoA desaturase (SCD) regulatory circuit to maintain lipid homeostasis.

MATERIALS AND METHODS

Strains and culture conditions

C. elegans strains were maintained on NGM plates with *Escherichia coli* OP50 under standard culture conditions, unless otherwise specified. The WT strain was N2. CB4856 is a WT isolated from Hawaii used for SNP mapping. The organisms and strains used in this study are shown in supplemental Table S1.

RNAi

RNAi was performed by feeding bacterial strains from the Ahringer *C. elegans* RNAi library, as we described previously (35). Young adult animals were harvested for further analysis.

Genome screening and isolation of *sbp-1* suppressors

Genome screening of *sbp-1(ep79)* suppressors was carried out following a previously described method (36, 37). Briefly, L4 *sbp-1(ep79)* worms were treated with ethyl methanesulfonate. Individual F2 worms that displayed morphologies of growth, body size, and color obviously close to the WT N2 were singled out and continuously cultured to the F3 generation. Then, F3 worms were harvested for analysis of fat accumulation by Nile red staining of fixed cells and analysis of fatty acid composition by GC, as well as quantification of the growth rate, to confirm the real suppressors of the *sbp-1(ep79)* mutant.

Mutation mapping by SNP markers and whole genome sequencing

Mutation mapping of *sbp-1(ep79)* suppressors (*kun82* and *kun84*) was carried out using snip-SNP, as previously described (38, 39). Whole genome sequencing (WGS) of *kun82;sbp-1(ep79)* and *kun84;sbp-1(ep79)* mutants was performed using the method of Sarin et al. (40). Briefly, the genomic DNA of *kun82;sbp-1(ep79)* and *kun84;sbp-1(ep79)* worms was isolated and subjected to WGS on the Illumina HiSeq2000 platform. The sequence data were mapped to the sequence of the WT N2 reference genome using ELAND via the BWA and SAMtools.

Nile red staining of fixed worms and quantification of lipid droplet size

Nile red staining of fixed worms was performed as previously described (28, 41). The images were captured using identical settings. At least 20 worms were visualized. The quantification of lipid droplet size was as previously described (42). Approximately six to eight worms were measured for each worm strain or treatment.

Analysis of fatty acid composition and triacylglycerol

C. elegans lipid extraction, the separation of triacylglycerol (TAG) and phospholipids by TLC, and the determination of fatty acids by GC were performed as previously described (42). Fatty acid compositions were analyzed with an Agilent 7890A gas chromatograph equipped with a 15 m × 0.25 mm × 0.25 μm DB-WAX column.

Analysis of quantitative real-time PCR and semi-quantitative PCR

Total RNA and cDNA preparation, quantitative real-time PCR (QPCR), and semi-QPCR were performed as previously described (43). For semi-quantitative PCR, there were 25 PCR cycles for *sbp-1*. For QPCR, the relative abundance was determined using the $\Delta\Delta C_t$ method and the reference gene, *act-5*, was used as a control for template levels.

Supplementation or sequestration of zinc

ZnSO₄ supplementation and zinc reduction by *N,N,N,N*-tetraakis (2-pyridylmethyl) ethylenediamine (TPEN) were analyzed as described previously (44, 45). In brief, ZnSO₄ and TPEN were added to NGM plates to a final concentration of 50 and 5 μM, respectively. Later, synchronized L1 worms were placed and cultivated on NGM plates supplied with either ZnSO₄ or TPEN. L4 worms or young adults were harvested for analysis.

Zinpyr-1 staining and visualization

Zinpyr-1 staining was performed as described previously (46). The fluorescence of Zinpyr-1 was visualized under an OLYMPUS BX53 fluorescence microscope (Olympus, Japan). Images were captured using identical settings and exposure times, unless specifically noted. The fluorescence intensity was quantified using Photoshop software.

Visualization of GFP fluorescence

At least 20 GFP worms were picked and mounted on an agarose pad and anesthetized using 10 mM sodium azide. GFP fluorescence was visualized under an OLYMPUS BX53 fluorescence microscope (Olympus, Japan). GFP reporter expression was quantified using Photoshop software. At least six worms were used for each biological sample.

Statistical analysis

The data were presented as the mean ± SEM, except when specifically indicated. Statistical analyses included the *t*-test or ANOVA. All figures were generated using GraphPad Prism 6 (GraphPad Software, La Jolla, CA).

RESULTS

Whole genome screen of genetic suppressors of *sbp-1(ep79)* mutant

Previously, we reported a reduction-of-function allele, *ep79*, of *sbp-1* encoding a homolog of SREBPs, which was created by the excision of a Tc1 element (supplemental

Fig. S1) (28). The *sbp-1(ep79)* mutant displayed decreased fat accumulation with reduced lipid droplet size compared to WT N2, as quantified by TLC/GC and indicated by our established Nile Red staining of fixed worms (supplemental Fig. S2A–C) (28, 41). There was a different fatty acid profile of the *sbp-1(ep79)* mutant, especially the levels of C18:0 and C18:1(n-9) (supplemental Fig. S2D), which led to the reduced conversion activity of SCD as indicated by the desaturation index C18:1(n-9)/C18:0 (supplemental Fig. S2E) (47). Moreover, the growth rate of *sbp-1(ep79)* was delayed (supplemental Fig. S2F). To identify genes or signaling pathways that might bypass SBP-1 to regulate lipid metabolism, we performed a forward genetic screen for suppressors of the *sbp-1(ep79)* mutant. We treated the *sbp-1(ep79)* mutant with the mutagen, ethyl methanesulfonate, and monitored the growth rate and lipid deposition using Nile red staining fixation and TLC/GC confirmation. We scored approximately 80,000 haploids and eventually isolated 10 suppressors named *kun64*, *kun70*, *kun72*, *kun78*, *kun79*, *kun81*, *kun82*, *kun83*, *kun84*, and *kun86*, which rescued the fat accumulation of *sbp-1(ep79)* to some extent (supplemental Fig. S3).

The top two mutations, *kun82* and *kun84*, significantly increased lipid droplet size and TAG content, restored the fatty acid profiles, and partially rescued the growth rate in the *sbp-1(ep79)* mutant background (Fig. 1). Therefore, they were chosen to identify the mutation in a specific gene by classical mapping of snip-SNP (38, 39) and WGS (40). Eventually, *kun82* was mapped to chromosome I and identified as a missense mutation in *smg-2* (GGT to GAT, G805D) (supplemental Fig. S4A), while *kun84* was mapped to chromosome X and identified as a missense mutation in *sur-7* (CCT to CTT, P191L) (Fig. 2A).

SMG-2 is an ortholog of human UPF1 (UPF1 regulator of nonsense transcripts in yeast) and is required for nonsense-mediated mRNA decay or mRNA surveillance (48, 49). Because *ep79* is a reduction-of-function allele of *sbp-1* (28), we thought that the *smg-2(kun82)* mutation might affect the mRNA expression of *sbp-1*. Indeed, QPCR and semi-QPCR showed that the mRNA expression level of *sbp-1* was obviously increased to the WT level in *sbp-1(ep79);smg-2(kun82)* mutants, but not in *sbp-1(ep79);sur-7(kun84)* mutants, compared with the *sbp-1(ep79)* single mutant alone (supplemental Fig. S4B, C). Therefore, increasing or stabilizing the expression of truncated *sbp-1* by mutation of *smg-2* may be able to restore its biological functions.

Inactivation of SUR-7 restores lipid profiles of *sbp-1(ep79)* mutant

The *sur-7* encodes a member of the CDF family (50, 51). At least two additional alleles, *tm6523* and *ku119*, of *sur-7* are available from Wormbase (<http://www.wormbase.org>). The *tm6523* mutation contains a 566 bp deletion, and *ku119* has a substitution mutation (GT-AT) near the 5' splicing site in the third intron that leads to an altered transcript (Fig. 2A, supplemental Fig. S5). To confirm the suppression of *sbp-1(ep79)* by *sur-7(kun84)*, we then crossed the *tm6523* and *ku119* alleles into the *sbp-1(ep79)* mutant

background, respectively. In accordance with the *kun84* mutation, both mutant alleles significantly increased lipid droplet size, fat content (TAG), the level of C18:1(n-9), and conversion activity of SCD, but decreased the level of C18:0, as well as improved the growth rates of the *sbp-1(ep79)* mutant (Fig. 2B–H). In addition, both *sur-7(tm6523)* and *sur-7(ku119)* mutants accumulated slightly, but significantly, higher fat contents than the WT (Fig. 2D), suggesting a slight difference among the three alleles of the *sur-7* gene. Because the phenotypes of *sur-7(tm6523)* and *sur-7(ku119)* mutants were similar (Fig. 2B–H), we then used *tm6523* and *kun84* mutations for the rest of the experiments for convenience. Meanwhile, unlike the *kun82* mutation of *smg-2* (supplemental Fig. S4B, C), mutations of *tm6523* and *kun84* did not affect the mRNA expression of *sbp-1* (supplemental Fig. S6), implying a distinct mechanism from SMG-2 to suppress the defects of the *sbp-1(ep79)* mutant. Taken together, these results indicate that disruption of SUR-7 apparently alleviates the defects of the *sbp-1(ep79)* mutant.

SBP-1 functions to reduce zinc level

SUR-7 was reported to likely localize to the endoplasmic reticulum membrane and play a role in zinc metabolism (46, 50), raising the question of whether SBP-1 has a role in zinc homeostasis. MTL-1, one of two *C. elegans* metallo-thioneins, was reported to have high zinc binding ability (52). In fact, the mRNA expression of *mtl-1* was very responsive to the zinc level, in which it was significantly induced by supplementation with ZnSO₄ or reduced by the zinc chelator, TPEN (Fig. 3A). Interestingly, the expression of *mtl-1* was significantly increased in the *sbp-1(ep79)* mutant, but was reversely inhibited in the *sur-7(tm6523)* and *sur-7(kun84)* mutants (Fig. 3B).

Zinpyr-1 fluorescence was used to measure labile zinc and the level of pseudocoelomic zinc (46). Both *sur-7(tm6523)* and *sur-7(kun84)* mutants displayed weaker Zinpyr-1 fluorescence than N2 under normal conditions (Control) (Fig. 3C, D). Surprisingly, compared with the WT (N2), the *sbp-1(ep79)* mutant displayed increased Zinpyr-1 fluorescence, but was repressed in both *sur-7(tm6523)* and *sur-7(kun84)* mutants (Fig. 3C, D). Meanwhile, TPEN treatment obviously abolished the Zinpyr-1 fluorescence in all strains (Fig. 3C, D). Interestingly, the mRNA expression of *sur-7* was not different between *sbp-1(ep79)* and N2 worms (Fig. 3E), suggesting that SBP-1 did not regulate the transcriptional expression of *sur-7*. Nevertheless, these data clearly indicate that SBP-1 negatively regulates zinc homeostasis and that the high level of zinc in the *sbp-1(ep79)* mutant requires the activity of SUR-7.

Zinc bypasses SBP-1 to negatively regulate fat accumulation

Because the Zinpyr-1 fluorescence was negatively correlated with fat accumulation in both *sbp-1* and *sur-7* mutants, we hypothesized that zinc might affect fat accumulation. Dietary supplementation with ZnSO₄ had no obvious effect on fat accumulation, indicated by Nile red staining of fixed worms and lipid droplet size in both N2 and *sbp-1(ep79)* worms (Fig. 3F, G). However, compared with the control,

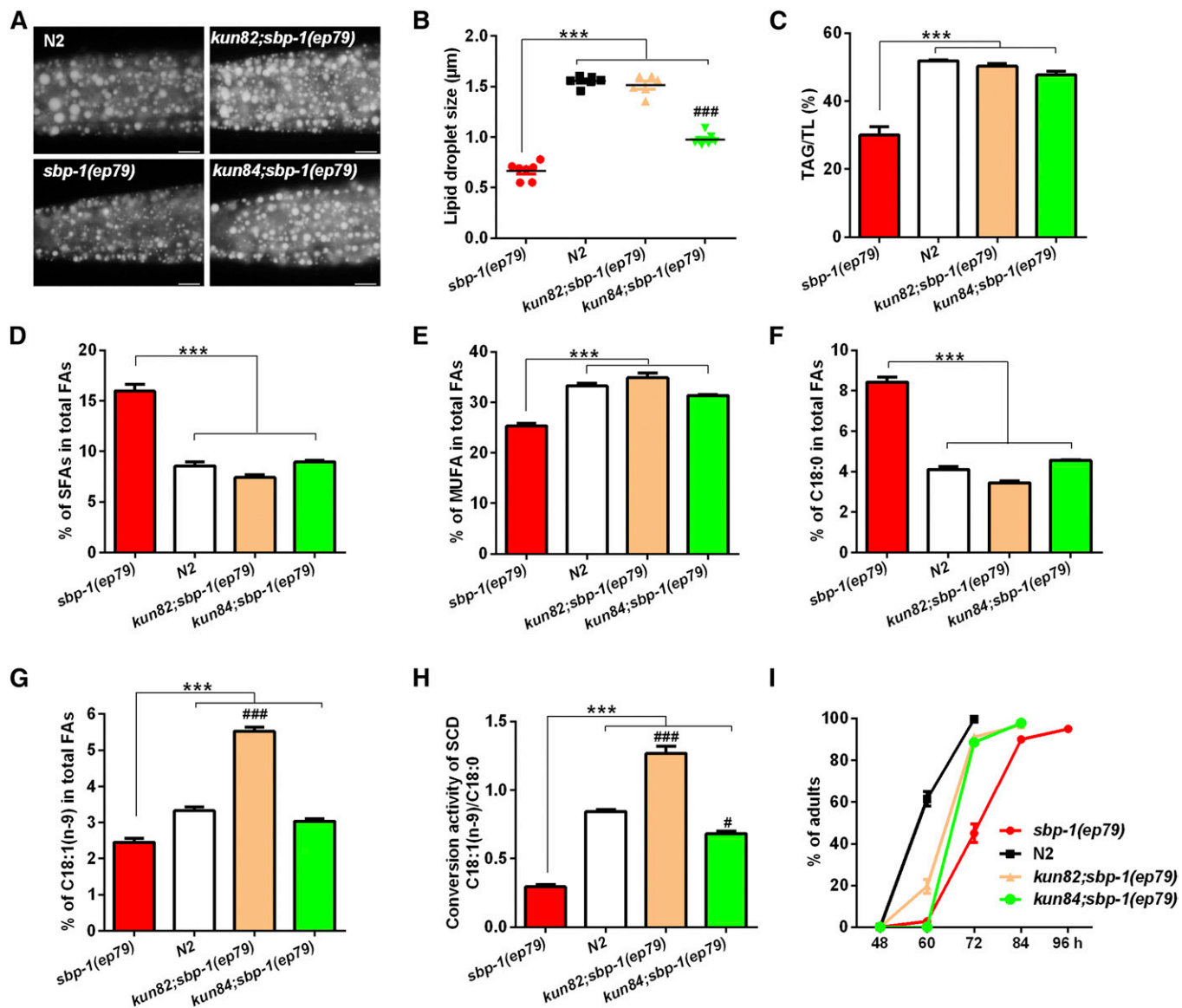


Fig. 1. The *kun82* and *kun84* mutations are suppressors of the *sbp-1(ep79)* mutant. A: Nile red staining of fixed worms. Representative animals, the anterior is on the right and the posterior is on the left. Scale bar represents 10 µm. B: Lipid droplet size in the posterior region of intestines from six to seven worms of each worm strain. The data are presented as scatter dot plot and mean. C: Percentage of TAG in total lipids (TAG/TL). The data are presented as the mean ± SEM of three to four biological repeats. D–G: Percentage of saturated fatty acids (SFAs) (C16:0 + C18:0) (D), MUFAs [C16:1(n-7) + C18:1(n-9) + C18:1(n-7)] (E), C18:0 (F), and C18:1(n-9) (G) in total fatty acids. The data are presented as the mean ± SEM of at least four biological repeats. H: The conversion activity of SCD presented as the ratio of C18:1(n-9)/C18:0. The data are presented as the mean ± SEM of four biological repeats. I: The growth rate of worms. The data are presented as the mean ± SEM of three biological repeats of which at least 300 worms were counted for each worm strain. Statistical analysis was performed using ANOVA. *** $P < 0.001$, significant difference between *sbp-1(ep79)* mutant and a specific worm strain. # $P < 0.05$, ### $P < 0.001$, significant difference between WT N2 and a specific worm strain.

ZnSO₄ treatment apparently reduced the fat accumulation and lipid droplet size in strains with a *sur-7* mutant background, including *sur-7(tm6523)*, *sur-7(tm6523);sbp-1(ep79)*, *sur-7(kun84)*, and *sur-7(kun84);sbp-1(ep79)* mutants (Fig. 3F, G). On the contrary, reduction of zinc by TPEN treatment remarkably exacerbated the fat accumulation and increased lipid droplet size in all tested strains (Fig. 3F, G). In brief, these data explicitly supported that zinc negatively affected fat accumulation, and the restored fat accumulation of the *sbp-1(ep79)* mutant was due to the reduction in zinc levels.

Zinc negatively regulates the activity of SCD, a main target of SREBP

SCD introduces the first double bond and converts saturated fatty acids (C16:0 and C18:0) to MUFAs [C16:1(n-7) and C18:1(n-9)], which are the primary substrates for the biosynthesis of TAGs, phospholipids, and cholesterol esters (53). SCD is a main target of SREBP, which transcriptionally regulates SCD expression from *C. elegans* to mammals (28, 53, 54). Although the expression of *sbp-1* was not affected in *sur-7(tm6523);sbp-1(ep79)* and *sur-7(kun84);sbp-1(ep79)* mutants, as in the *sbp-1(ep79)* mutant alone

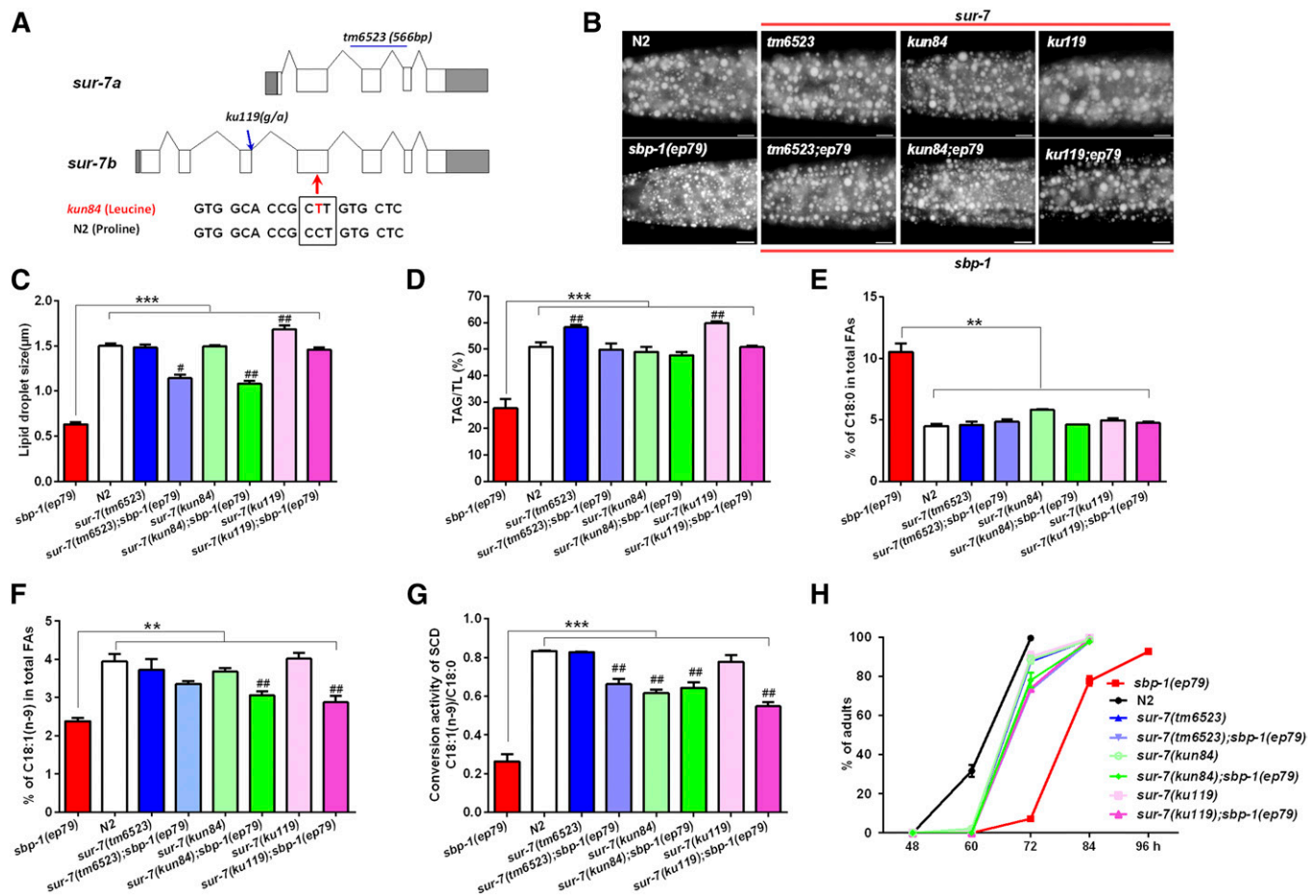


Fig. 2. All three mutations of *sur-7* successfully rescue the lipid profile and growth rate of the *sbp-1(ep79)* mutant. A: The structure diagram of the *sur-7* gene and three alleles. The *kun84* is a missense mutation (P191L) in the fourth exon, the *tm6523* mutation has a 566 bp deletion, and *ku119* is a substitution mutation (GT→AT) neighboring the splicing site. B: Nile red staining of fixed worms. Representative animals, the anterior is on the right and the posterior is on the left. Scale bar represents 10 μm. C: Lipid droplet size in the posterior region of intestines from eight worms of each worm strain. The data are presented as mean ± SEM. D: Percentage of TAG in total lipids (TAG/TL). The data are presented as the mean ± SEM of four biological repeats. E, F: Percentage of C18:0 (E) and C18:1(n-9) (F) in total fatty acids. The data are presented as the mean ± SEM of four biological repeats. G: The conversion activity of SCD presented as the ratio of C18:1(n-9)/C18:0. The data are presented as the mean ± SEM of four biological repeats. H: The growth rate of worms. The data are presented as the mean ± SEM of three biological repeats of which at least 300 worms were counted for each worm strain. Statistical analysis was performed using ANOVA. ** $P < 0.01$, *** $P < 0.001$, significant difference between *sbp-1(ep79)* mutant and a specific worm strain. # $P < 0.05$, ## $P < 0.01$, significant difference between WT N2 and a specific worm strain.

(supplemental Fig. S6), the level of C18:1(n-9) (Fig. 2F), which is the de novo synthesized fatty acid by SCD in *C. elegans* (54, 55), and the conversion activity of SCD were significantly elevated in *sur-7;sbp-1* double mutants compared with the *sbp-1(ep79)* mutant (Fig. 2G), implying a mechanism independent of SBP-1 transcription to regulate SCD conversion activity. In fact, dietary ZnSO₄ slightly, but significantly, decreased both the level of C18:1(n-9) and the conversion activity of SCD (Fig. 4A, B) in the *sur-7* mutant background. In contrast, zinc reduction by TPEN treatment dramatically increased the C18:1(n-9) level and the conversion activity of SCD in all tested strains except the *fat-6(tm331);fat-7(wa37)* mutants (Fig. 4A, B), which lack SCD enzymes for the conversion of C18:0 to C18:1(n-9) in *C. elegans* (54). Altogether, these results suggest that the suppression of the *sbp-1(ep79)* mutant is due to increased conversion activity of SCD and its converted product, C18:1(n-9). Furthermore, dietary supplementation with

oleic acid [C18:1(n-9)] improved fat accumulation with increased lipid droplet size and the growth rate in the *sbp-1(ep79)* mutant (supplemental Fig. S7), which was consistent with a previous report (32).

To examine whether the increased level of C18:1(n-9) and SCD conversion activity by TPEN treatment was due to upregulated expression of *scds*, we investigated the mRNA and GFP expression of *fat-5*, *fat-6*, and *fat-7*, encoding three separate SCDs, in *C. elegans* (54). Interestingly, the GFP expression of all three SCDs and the mRNA expression of *fat-5* and *fat-7* were significantly reduced in TPEN-treated worms compared with the control worms, while ZnSO₄ treatment slightly, but significantly, increased the fluorescence intensity of FAT-6::GFP and FAT-7::GFP (Fig. 4C–E). Moreover, TPEN treatment obviously reduced the GFP expression of GFP::SBP-1 (KQ377) in the nucleus compared with the control (Fig. 4F), whereas it did not affect the mRNA expression of *sbp-1* (Fig. 4G). Therefore, zinc reduction

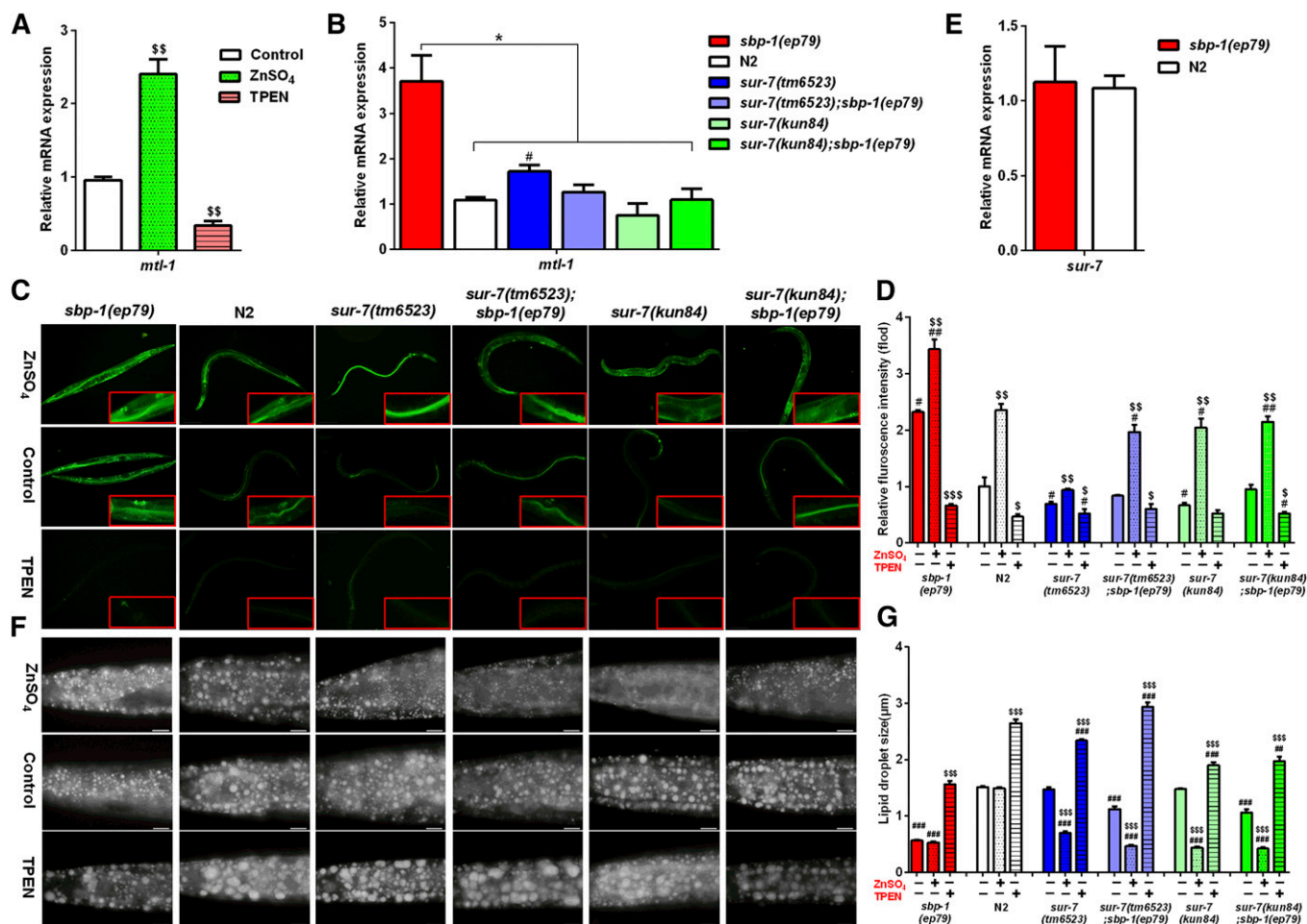


Fig. 3. SBP-1 negatively regulates zinc level. **A, B:** Relative mRNA expression of *mtl-1* by QPCR. The data are presented as the mean \pm SEM of three to four biological repeats. **C:** Fluorescence microscopy of live animals stained with Zinpyr-1. Scale bar represents 100 μ m for the whole animal and 20 μ m for the enlarged body part, respectively. Images were captured using identical settings and exposure times. **D:** Quantitation of the fluorescence intensity from (C). The data are presented as the mean \pm SEM from three worms of each worm strain. **E:** Relative mRNA expression of *sur-7* by QPCR. The data are presented as the mean \pm SEM of four biological repeats. **F:** Nile red staining of fixed worms. Representative animals, the anterior is on the right and posterior is on the left. Scale bar represents 10 μ m. **G:** Lipid droplet size in the posterior region of intestines from eight worms of each worm strain. The data are presented as mean \pm SEM. The concentration of TPEN is 5 μ M and of ZnSO₄ is 50 μ M. Statistical analysis was performed using the *t*-test. #*P* < 0.05, ##*P* < 0.01, ###*P* < 0.001, significant difference between WT N2 and a specific condition. \$*P* < 0.05, \$\$*P* < 0.01, \$\$\$*P* < 0.001, significant difference between the control and either TPEN treatment or ZnSO₄ treatment. **P* < 0.05, significant difference between a specific worm strain and *sbp-1(ep79)* mutant.

might repress the nuclear translocation of SBP-1 and then downregulate the transcriptional and translational expression of *scds*. However, these results were contradicted by the increased level of C18:1(n-9) and the conversion activity of SCD (Fig. 4A, B).

In spite of that, RNAi knockdown of *fat-6*, which had a stronger RNAi effect than *fat-7* RNAi to some degree, apparently decreased fat accumulation with decreased lipid droplet size in all test strains (Fig. 4H, J), even under TPEN treatment (Fig. 4I, K). In addition, although the *fat-6(tm331);fat-7(wa37)* double mutants were similar to the *sbp-1(ep79)* mutant in terms of fat accumulation, they were partially resistant to TPEN-induced fat accumulation (Fig. 4L, M). Altogether, these results suggest that zinc reduction-induced fat accumulation probably depends on the SCD function, in which its conversion activity was elevated, but its transcriptional and translational expression was repressed inversely.

Zinc antagonizes iron to determine SCD conversion activity and fat accumulation

To explore genes responding to zinc reduction, we performed RNA-seq analysis in worms treated with 2.5 and 5 μ M TPEN. Transcriptome profiles revealed that the expression of 78 genes was responsive to TPEN in a concentration-dependent manner (Fig. 5A, B; supplemental Table S2). Consistent with our previous QPCR results (Fig. 4E), the expression of *fat-5* and *fat-7* was also downregulated in the RNA-seq data (Fig. 5B). Surprisingly, we found that the expression of *ftn-1* and *smf-3*, encoding ferritin and divalent metal-ion transporter 1 (DMT1), respectively, was reversely responsive to zinc concentration. Previous reports, including ours, show that the expression of the *ftn-1* gene and protein are induced; in contrast, the expression of *smf-3* is suppressed to reduce iron uptake under iron overload (56–58). QPCR confirmed that the mRNA expression of *ftn-1* and *smf-3* indeed displayed an opposite pattern in

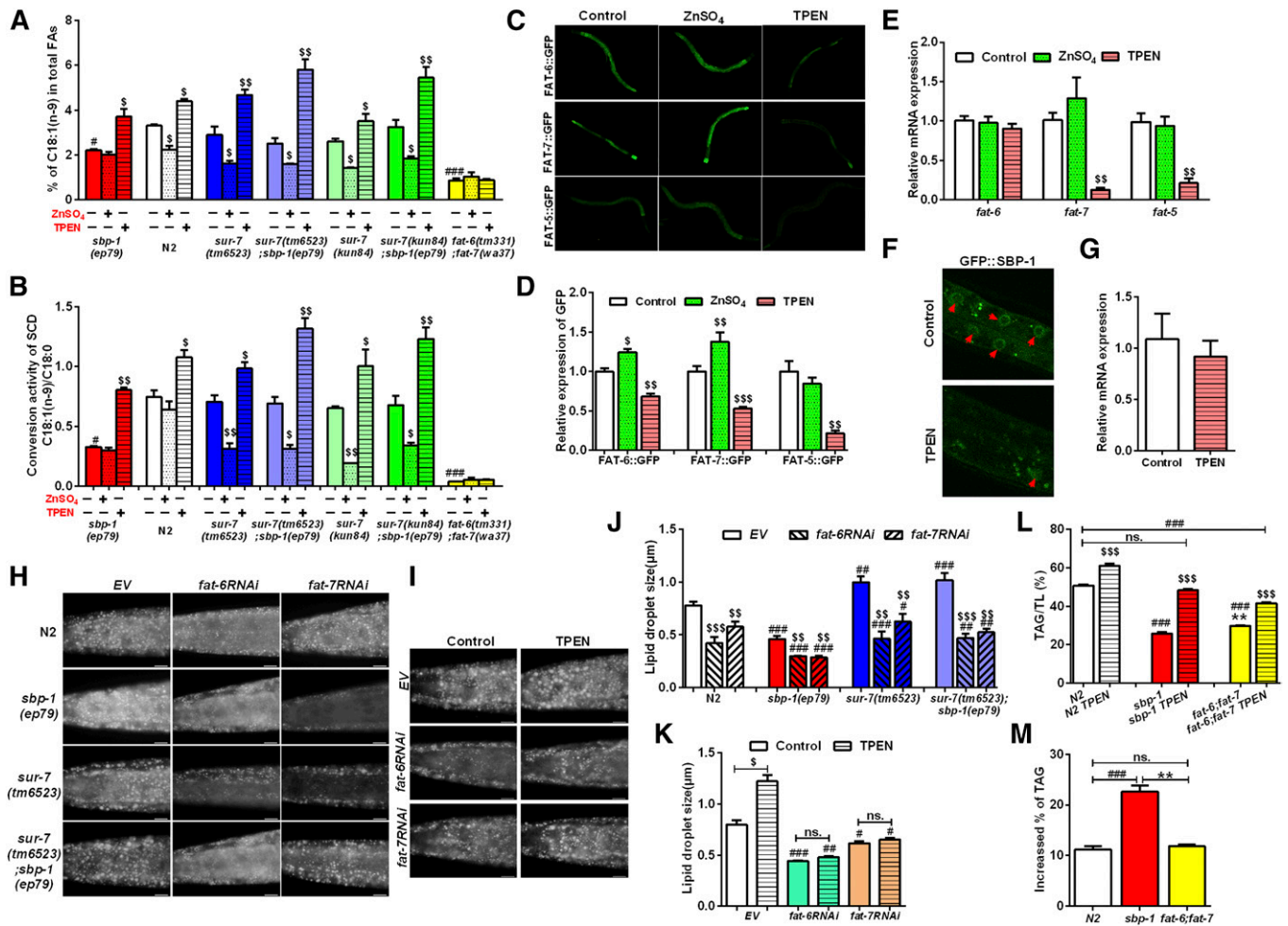


Fig. 4. Zinc reduction increases the conversion activity of SCD. **A:** Percentage of C18:1(n-9) in total fatty acids. The data are presented as the mean \pm SEM of three to four biological repeats. **B:** The conversion activity of SCD presented as the ratio of C18:1(n-9)/C18:0. The data are presented as the mean \pm SEM of three to four biological repeats. **C:** Fluorescence microscopy of FAT-5::GFP, FAT-6::GFP, and FAT-7::GFP. Scale bar represents 100 μ m. The concentration of TPEN is 5 μ M and of ZnSO₄ is 200 μ M. Images were captured using identical settings and exposure times. **D:** Quantitation of the fluorescence intensity from (C). The data are presented as the mean \pm SEM. At least five worms were analyzed for each treatment. **E:** Relative mRNA expression of *fat-5*, *fat-6*, and *fat-7* by QPCR. The data are presented as the mean \pm SEM of four biological repeats. Statistical analysis was performed using the *t*-test. **F:** Fluorescence intensity of GFP::SBP-1 (KQ377) treated by TPEN. The red arrows indicate nuclear. Images were captured by confocal microscopy using identical settings and exposure times. **G:** Relative mRNA expression of *sbp-1* by QPCR. The data are presented as the mean \pm SEM of four biological repeats. **H, I:** Nile red staining of fixed worms. Representative animals, the anterior is on the right and the posterior is on the left. Scale bar represents 10 μ m. **J, K:** Lipid droplet size in the posterior region of intestines from four worms of each condition. The data are presented as mean \pm SEM. **L:** Percentage of TAG in total lipids (TAG/TL). The data are presented as the mean \pm SEM of four biological repeats. **M:** The increased percentage of TAG between TPEN treatment and nontreatment in a specific worm strain. The data are presented as the mean \pm SEM of four biological repeats. The concentration of TPEN is 5 μ M and of ZnSO₄ is 50 μ M. The statistical analysis was performed using ANOVA unless specifically indicated. #*P* < 0.05, ##*P* < 0.01, ###*P* < 0.001, significant difference between WT (N2) and a specific worm strain. ***P* < 0.01, significant difference between a specific worm strain and *sbp-1(ep79)* mutant. \$*P* < 0.05, \$\$*P* < 0.01, \$\$\$*P* < 0.001, significant difference between treatment (TPEN or ZnSO₄) and nontreatment (Control) in the same worm strain. ns., no significant difference between the two groups.

response to zinc concentrations (Fig. 5C, D). Consistently, TPEN treatment dramatically increased the fluorescent expression of FTN-1::GFP, while dietary ZnSO₄ had a negative effect (Fig. 5E). Thus, zinc had an antagonizing role to affect iron homeostasis.

SCDs are iron-containing enzymes that require iron for their activity (53, 59). Because zinc reduction increased FTN-1 expression and SCD conversion activity, we hypothesized that the elevated conversion activity of SCD by zinc reduction was probably due to iron overload. The iron chelator, 2,2'-dipyridyl (BP), was used to reduce the iron level (60). Indeed, the level of C18:0 was increased and the

conversion activity of SCD was decreased in a BP concentration-dependent manner (Fig. 5F, G). However, TPEN treatment significantly increased the level of C18:1(n-9) and the conversion activity of SCD, even under BP treatment (Fig. 5F, G). Although either TPEN or BP treatment apparently reduced the growth rate of worms, TPEN treatment obviously improved the slow growth rate of worms treated with BP (Fig. 5H). In addition, compared with the control, TPEN treatment led to high fat accumulation with increased lipid droplet size, while BP treatment had the opposite effect in worms (Fig. 5I, J). Moreover, TPEN treatment restored the low level of fat accumulation in

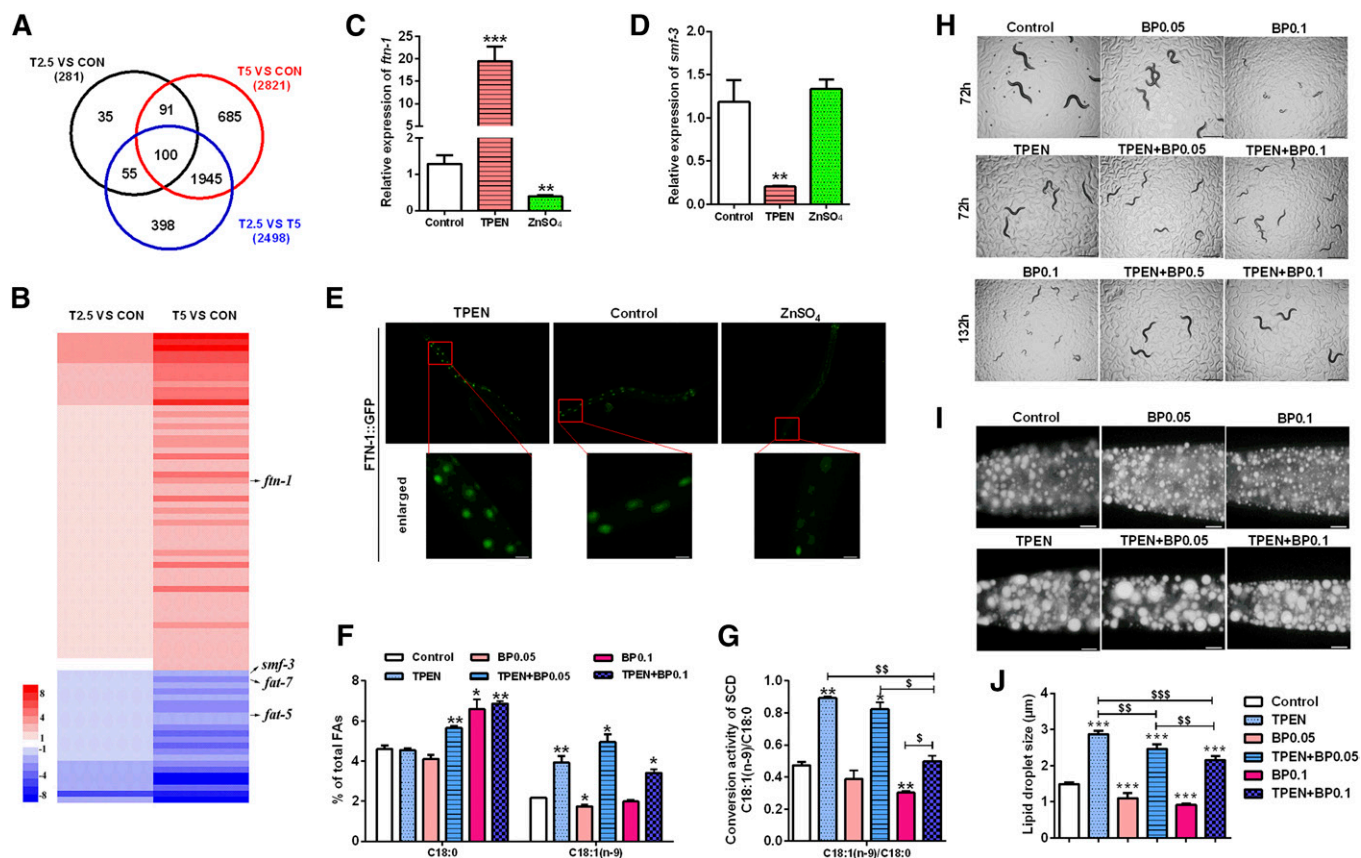


Fig. 5. Iron antagonizes zinc to regulate the conversion activity of SCD and fat accumulation. **A:** The number of differentially expressed genes among TPEN (T, 2.5 or 5 μ M) treatments and nontreatment (CON) in WT (N2) by transcriptome analysis. **B:** Heat map of 78 differentially expressed genes responsive to TPEN concentrations. The cutoff line is 1.4-fold different between TPEN treatment (T, 2.5 or 5 μ M) and nontreatment (CON). **C, D:** Relative mRNA expression of *fnr-1* (C) and *smf-3* (D) by QPCR. The data are presented as the mean \pm SEM of three to four biological repeats. **E:** Fluorescence microscopy of FTN-1::GFP [XA6900 (*P_{ftn-1}::pes-10::GFP-his*)]. Scale bar represents 100 μ m. **F:** Percentage of C18:0 and C18:1 (n-9) in total fatty acids. The data are presented as the mean \pm SEM of three to four biological repeats. **G:** The conversion activity of SCD presented as the ratio of C18:1 (n-9)/C18:0. The data are presented as the mean \pm SEM of at least three to four biological repeats. **H:** The light field of the growth of WT N2 worms under different treatments. Synchronized L1 worms were cultured on NGM plates containing TPEN (5 μ M) or BP (0.1 or 0.05 μ M) at 0 h, and the photographs were taken at 72 or 132 h. Scale bar represents 500 μ m. **I:** Nile red staining of fixed worms. Representative animals, the anterior is on the right and the posterior is on the left. Synchronized L1 worms were cultured on NGM plates containing TPEN (5 μ M) or BP (0.1 or 0.05 μ M), harvested, and stained when they reached adulthood. Scale bar represents 10 μ m. **J:** Lipid droplet size in the posterior region of intestines from six worms of each condition. The data are presented as mean \pm SEM. Statistical analyses were performed using the *t*-test (F, G, J) or ANOVA (C, D). * P < 0.05, ** P < 0.01, *** P < 0.001, significant difference between treatment (TPEN or BP) and nontreatment (Control). $^{\$}$ P < 0.05, $^{\$\$}$ P < 0.01, $^{\$ \$ \$}$ P < 0.001, significant difference between two indicated treatments (either TPEN or BP).

BP-treated worms (Fig. 5I, J). Altogether, these lines of evidence consistently suggest that iron competes with zinc to determine the SCD conversion activity and fat accumulation, and zinc reduction-induced fat accumulation depends on the iron-activated SCD conversion activity.

DISCUSSION

The evolutionarily conserved transcription factors, SREBPs, play central roles to transcriptionally regulate genes involved in fatty acid, triglyceride, and cholesterol metabolism, from *C. elegans* to mammals. To our great surprise, we found that the *sbp-1(ep79)* mutant displayed an elevated zinc level, as indicated by Zinpyr-1 fluorescence and *mtl-1* expression (Fig. 3A–D). In contrast, zinc reduction repressed the nuclear translocation of GFP::SBP-1 (Fig. 4F), consequently downregulating the transcriptional expression

of the *scd* genes, *fat-5*, *fat-6*, and *fat-7* (Fig. 4C–E). Furthermore, zinc was sufficient to directly regulate SCD function and lipid homeostasis, independent of SREBP function (Fig. 6). Thus, we uncovered a distinct zinc-mediated regulation of SREBP-SCD in lipid metabolism, in which SREBP repressed the zinc level to upregulate SCD conversion activity, while, reciprocally, zinc affected the transactivation of SREBP on *scd* genes (Fig. 6), although the details need to be further characterized.

SCD1 catalysis is dependent on its di-iron center (53, 61). Interestingly, the recent crystal structure of mouse SCD1 showed that zinc, instead of iron, was the predominant ion in the structure (62). We found that zinc reduction led to iron overload, as well as increased SCD conversion activity and fat accumulation, consistent with a recent report that zinc deficiency promotes insulin resistance by exacerbating iron overload in the liver and induces hepatic steatosis in patients (63). On the other hand,

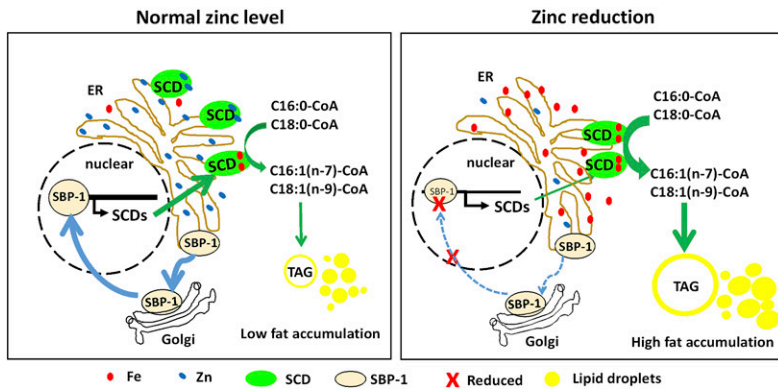



Fig. 6. A working model of how zinc mediates the SBP-1-SCD axis to regulate lipid metabolism. Under normal zinc level, zinc promotes SBP-1 (SREBP homolog) nuclear translocation to transcriptionally regulate SCD expression, whereas zinc competitively replaces iron to inactivate the enzymatic activity of SCD to reduce biosynthesis of MUFAs and maintain normal fat accumulation. In contrast, zinc reduction leads to the removal of zinc from the SCD enzyme, allowing iron to incorporate into SCD to directly activate its catalyzing function, promoting the biosynthesis of MUFAs and fat accumulation. Zinc reduction may feed back to repress the nuclear translocation of SBP-1 and reduces its transcriptional activation of SCD.

the reduction of iron by BP indeed decreased the SCD conversion activity and fat accumulation, whereas it was absolutely reversed by zinc reduction (Fig. 5F–J). Thus, our results, together with those of others, convincingly revealed an evolutionarily antagonistic role between zinc and iron to determine SCD conversion activity and fat accumulation from *C. elegans* to humans.

Zinc has been reported to play an important role in lipid metabolism. The zinc content was significantly lower in patients with alcoholic liver disease (64). In contrast, zinc supplementation significantly reduced total cholesterol, LDL cholesterol, and triglycerides in a meta-analysis of 24 studies on humans (65) and reversed alcoholic steatosis in mice (66). Here, we showed that zinc reduction promoted SCD conversion activity, but increased levels of zinc conversely impaired SCD conversion activity to positively or negatively affected fat accumulation in *C. elegans* (Fig. 6). Altogether, these results revealed an evolutionarily conserved role of zinc that negatively regulated fat accumulation, from *C. elegans* to humans. Reduction in iron or targeting SCD may hold potential promise for the treatment of zinc- or iron-related metabolic diseases. 

Some strains were provided by the CGC, which is funded by National Institutes of Health Office of Research Infrastructure Program.

REFERENCES

- Goldstein, J. L., R. A. DeBose-Boyd, and M. S. Brown. 2006. Protein sensors for membrane sterols. *Cell*. **124**: 35–46.
- Horton, J. D., J. L. Goldstein, and M. S. Brown. 2002. SREBPs: activators of the complete program of cholesterol and fatty acid synthesis in the liver. *J. Clin. Invest.* **109**: 1125–1131.
- Raghow, R., C. Yellaturu, X. Deng, E. A. Park, and M. B. Elam. 2008. SREBPs: the crossroads of physiological and pathological lipid homeostasis. *Trends Endocrinol. Metab.* **19**: 65–73.
- Jeon, T. I., and T. F. Osborne. 2012. SREBPs: metabolic integrators in physiology and metabolism. *Trends Endocrinol. Metab.* **23**: 65–72.
- Shao, W., and P. J. Espenshade. 2012. Expanding roles for SREBP in metabolism. *Cell Metab.* **16**: 414–419.
- Brown, M. S., and J. L. Goldstein. 1997. The SREBP pathway: regulation of cholesterol metabolism by proteolysis of a membrane-bound transcription factor. *Cell*. **89**: 331–340.
- Walker, A. K., R. L. Jacobs, J. L. Watts, V. Rottiers, K. Jiang, D. M. Finnegan, T. Shioda, M. Hansen, F. Yang, L. J. Niebergall, et al. 2011. A conserved SREBP-1/phosphatidylcholine feedback circuit regulates lipogenesis in metazoans. *Cell*. **147**: 840–852.
- Goldstein, J. L., and M. S. Brown. 2015. A century of cholesterol and coronaries: from plaques to genes to statins. *Cell*. **161**: 161–172.
- Bi, Y., W. Wu, J. Shi, H. Liang, W. Yin, Y. Chen, S. Tang, S. Cao, M. Cai, S. Shen, et al. 2014. Role for sterol regulatory element binding protein-1c activation in mediating skeletal muscle insulin resistance via repression of rat insulin receptor substrate-1 transcription. *Diabetologia*. **57**: 592–602.
- Wang, H., P. Maechler, P. A. Antinozzi, L. Herrero, K. A. Hagenfeldt-Johansson, A. Bjorklund, and C. B. Wollheim. 2003. The transcription factor SREBP-1c is instrumental in the development of beta-cell dysfunction. *J. Biol. Chem.* **278**: 16622–16629.
- Vergès, B. 2005. New insight into the pathophysiology of lipid abnormalities in type 2 diabetes. *Diabetes Metab.* **31**: 429–439.
- Shimomura, I., Y. Bashmakov, and J. D. Horton. 1999. Increased levels of nuclear SREBP-1c associated with fatty livers in two mouse models of diabetes mellitus. *J. Biol. Chem.* **274**: 30028–30032.
- Kakuma, T., Y. Lee, M. Higa, Z. Wang, W. Pan, I. Shimomura, and R. H. Unger. 2000. Leptin, troglitazone, and the expression of sterol regulatory element binding proteins in liver and pancreatic islets. *Proc. Natl. Acad. Sci. USA*. **97**: 8536–8541.
- Laudes, M., I. Barroso, J. Luan, M. A. Soos, G. Yeo, A. Meirhaeghe, L. Logie, A. Vidal-Puig, A. J. Schafer, N. J. Wareham, et al. 2004. Genetic variants in human sterol regulatory element binding protein-1c in syndromes of severe insulin resistance and type 2 diabetes. *Diabetes*. **53**: 842–846.
- Eberlé, D., K. Clément, D. Meyre, M. Sahbatou, M. Vaxillaire, A. Le Gall, P. Ferré, A. Basdevant, P. Froguel, and F. Foufelle. 2004. SREBF-1 gene polymorphisms are associated with obesity and type 2 diabetes in French obese and diabetic cohorts. *Diabetes*. **53**: 2153–2157.
- Felder, T. K., H. Oberkofler, R. Weitgasser, V. Mackevics, F. Krempler, B. Paulweber, and W. Patsch. 2007. The SREBF-1 locus is associated with type 2 diabetes and plasma adiponectin levels in a middle-aged Austrian population. *Int. J. Obes. (Lond)*. **31**: 1099–1103.
- Laaksonen, R., K. M. Thelen, H. Paiva, J. Matinheikki, R. Vesalainen, T. Janatuinen, J. Knuuti, R. Rontu, K. von Bergmann, D. Lutjohann, et al. 2006. Genetic variant of the SREBF-1 gene is significantly related to cholesterol synthesis in man. *Atherosclerosis*. **185**: 206–209.
- Salek, L., S. Lutucuta, C. M. Ballantyne, A. M. Gotto, Jr., and A. J. Marian. 2002. Effects of SREBF-1a and SCAP polymorphisms on plasma levels of lipids, severity, progression and regression of coronary atherosclerosis and response to therapy with fluvastatin. *J. Mol. Med.* **80**: 737–744.
- Shimano, H., J. D. Horton, R. E. Hammer, I. Shimomura, M. S. Brown, and J. L. Goldstein. 1996. Overproduction of cholesterol and fatty acids causes massive liver enlargement in transgenic mice expressing truncated SREBP-1a. *J. Clin. Invest.* **98**: 1575–1584.
- Shimano, H., J. D. Horton, I. Shimomura, R. E. Hammer, M. S. Brown, and J. L. Goldstein. 1997. Isoform 1c of sterol regulatory element binding protein is less active than isoform 1a in livers of transgenic mice and in cultured cells. *J. Clin. Invest.* **99**: 846–854.
- Shimano, H., I. Shimomura, R. E. Hammer, J. Herz, J. L. Goldstein, M. S. Brown, and J. D. Horton. 1997. Elevated levels of SREBP-2 and cholesterol synthesis in livers of mice homozygous for a targeted disruption of the SREBP-1 gene. *J. Clin. Invest.* **100**: 2115–2124.
- Ishikawa, M., Y. Iwasaki, S. Yatoh, T. Kato, S. Kumadaki, N. Inoue, T. Yamamoto, T. Matsuzaka, Y. Nakagawa, N. Yahagi, et al. 2008. Cholesterol accumulation and diabetes in pancreatic beta-cell-specific SREBP-2 transgenic mice: a new model for lipotoxicity. *J. Lipid Res.* **49**: 2524–2534.
- Knebel, B., J. Haas, S. Hartwig, S. Jacob, C. Kollmer, U. Nitzgen, D. Muller-Wieland, and J. Kotzka. 2012. Liver-specific expression of

- transcriptionally active SREBP-1c is associated with fatty liver and increased visceral fat mass. *PLoS One*. **7**: e31812.
24. Takahashi, A., K. Motomura, T. Kato, T. Yoshikawa, Y. Nakagawa, N. Yahagi, H. Sone, H. Suzuki, H. Toyoshima, N. Yamada, et al. 2005. Transgenic mice overexpressing nuclear SREBP-1c in pancreatic beta-cells. *Diabetes*. **54**: 492–499.
 25. Horton, J. D., N. A. Shah, J. A. Warrington, N. N. Anderson, S. W. Park, M. S. Brown, and J. L. Goldstein. 2003. Combined analysis of oligonucleotide microarray data from transgenic and knockout mice identifies direct SREBP target genes. *Proc. Natl. Acad. Sci. USA*. **100**: 12027–12032.
 26. Horton, J. D., I. Shimomura, S. Ikemoto, Y. Bashmakov, and R. E. Hammer. 2003. Overexpression of sterol regulatory element-binding protein-1a in mouse adipose tissue produces adipocyte hypertrophy, increased fatty acid secretion, and fatty liver. *J. Biol. Chem.* **278**: 36652–36660.
 27. Dobrosotskaya, I. Y., A. C. Seegmiller, M. S. Brown, J. L. Goldstein, and R. B. Rawson. 2002. Regulation of SREBP processing and membrane lipid production by phospholipids in *Drosophila*. *Science*. **296**: 879–883.
 28. Liang, B., K. Ferguson, L. Kadyk, and J. L. Watts. 2010. The role of nuclear receptor NHR-64 in fat storage regulation in *Caenorhabditis elegans*. *PLoS One*. **5**: e9869.
 29. McKay, R. M., J. P. McKay, L. Avery, and J. M. Graff. 2003. *C. elegans*: a model for exploring the genetics of fat storage. *Dev. Cell*. **4**: 131–142.
 30. Kniazeva, M., T. Euler, and M. Han. 2008. A branched-chain fatty acid is involved in post-embryonic growth control in parallel to the insulin receptor pathway and its biosynthesis is feedback-regulated in *C. elegans*. *Genes Dev.* **22**: 2102–2110.
 31. Nomura, T., M. Horikawa, S. Shimamura, T. Hashimoto, and K. Sakamoto. 2010. Fat accumulation in *Caenorhabditis elegans* is mediated by SREBP homolog SBP-1. *Genes Nutr.* **5**: 17–27.
 32. Yang, F., B. W. Vought, J. S. Satterlee, A. K. Walker, Z. Y. Jim Sun, J. L. Watts, R. DeBeaumont, R. M. Saito, S. G. Hyberts, S. Yang, et al. 2006. An ARC/Mediator subunit required for SREBP control of cholesterol and lipid homeostasis. *Nature*. **442**: 700–704.
 33. Walker, A. K., F. Yang, K. Jiang, J. Y. Ji, J. L. Watts, A. Purushotham, O. Boss, M. L. Hirsch, S. Ribich, J. J. Smith, et al. 2010. Conserved role of SIRT1 orthologs in fasting-dependent inhibition of the lipid/cholesterol regulator SREBP. *Genes Dev.* **24**: 1403–1417.
 34. Kniazeva, M., Q. T. Crawford, M. Seiber, C. Y. Wang, and M. Han. 2004. Monomethyl branched-chain fatty acids play an essential role in *Caenorhabditis elegans* development. *PLoS Biol.* **2**: E257.
 35. Zhang, Y., X. Zou, Y. Ding, H. Wang, X. Wu, and B. Liang. 2013. Comparative genomics and functional study of lipid metabolic genes in *Caenorhabditis elegans*. *BMC Genomics*. **14**: 164.
 36. Jorgensen, E. M., and S. E. Mango. 2002. The art and design of genetic screens: *Caenorhabditis elegans*. *Nat. Rev. Genet.* **3**: 356–369.
 37. Brenner, S. 1974. Genetics of *Caenorhabditis elegans*. *Genetics*. **77**: 71–94.
 38. Davis, M. W., M. Hammarlund, T. Harrach, P. Hullett, S. Olsen, and E. M. Jorgensen. 2005. Rapid single nucleotide polymorphism mapping in *C. elegans*. *BMC Genomics*. **6**: 118.
 39. Wicks, S. R., R. T. Yeh, W. R. Gish, R. H. Waterston, and R. H. Plasterk. 2001. Rapid gene mapping in *Caenorhabditis elegans* using a high density polymorphism map. *Nat. Genet.* **28**: 160–164.
 40. Sarin, S., S. Prabhu, M. M. O'Meara, I. Pe'er, and O. Hobert. 2008. *Caenorhabditis elegans* mutant allele identification by whole-genome sequencing. *Nat. Methods*. **5**: 865–867.
 41. Brooks, K. K., B. Liang, and J. L. Watts. 2009. The influence of bacterial diet on fat storage in *C. elegans*. *PLoS One*. **4**: e7545.
 42. Shi, X., J. Li, X. Zou, J. Greggain, S. V. Rodkaer, N. J. Faergeman, B. Liang, and J. L. Watts. 2013. Regulation of lipid droplet size and phospholipid composition by stearoyl-CoA desaturase. *J. Lipid Res.* **54**: 2504–2514.
 43. Ding, Y., X. Zou, X. Jiang, J. Wu, Y. Zhang, D. Chen, and B. Liang. 2015. Pu-erh tea down-regulates sterol regulatory element-binding protein and stearoyl-CoA desaturase to reduce fat storage in *Caenorhabditis elegans*. *PLoS One*. **10**: e0113815.
 44. Bruinsma, J. J., D. L. Schneider, D. E. Davis, and K. Kornfeld. 2008. Identification of mutations in *Caenorhabditis elegans* that cause resistance to high levels of dietary zinc and analysis using a genomewide map of single nucleotide polymorphisms scored by pyrosequencing. *Genetics*. **179**: 811–828.
 45. Roh, H. C., S. Collier, J. Guthrie, J. D. Robertson, and K. Kornfeld. 2012. Lysosome-related organelles in intestinal cells are a zinc storage site in *C. elegans*. *Cell Metab.* **15**: 88–99.
 46. Roh, H. C., S. Collier, K. Deshmukh, J. Guthrie, J. D. Robertson, and K. Kornfeld. 2013. *tm-1* encodes CDF transporters that excrete zinc from intestinal cells of *C. elegans* and act in a parallel negative feedback circuit that promotes homeostasis. *PLoS Genet.* **9**: e1003522.
 47. Attie, A. D., R. M. Krauss, M. P. Gray-Keller, A. Brownlie, M. Miyazaki, J. J. Kastelein, A. J. Lusis, A. F. Stalenhoef, J. P. Stoehr, M. R. Hayden, et al. 2002. Relationship between stearoyl-CoA desaturase activity and plasma triglycerides in human and mouse hypertriglyceridemia. *J. Lipid Res.* **43**: 1899–1907.
 48. Page, M. F., B. Carr, K. R. Anders, A. Grimson, and P. Anderson. 1999. SMG-2 is a phosphorylated protein required for mRNA surveillance in *Caenorhabditis elegans* and related to Upf1p of yeast. *Mol. Cell. Biol.* **19**: 5943–5951.
 49. Johns, L., A. Grimson, S. L. Kuchma, C. L. Newman, and P. Anderson. 2007. *Caenorhabditis elegans* SMG-2 selectively marks mRNAs containing premature translation termination codons. *Mol. Cell. Biol.* **27**: 5630–5638.
 50. Yoder, J. H., H. R. Chong, K. L. Guan, and M. Han. 2004. Modulation of KSR activity in *Caenorhabditis elegans* by Zn ions, PAR-1 kinase and PP2A phosphatase. *EMBO J.* **23**: 111–119.
 51. Davis, D. E., H. C. Roh, K. Deshmukh, J. J. Bruinsma, D. L. Schneider, J. Guthrie, J. D. Robertson, and K. Kornfeld. 2009. The cation diffusion facilitator gene *cdf-2* mediates zinc metabolism in *Caenorhabditis elegans*. *Genetics*. **182**: 1015–1033.
 52. Zeitoun-Ghandour, S., J. M. Charnock, M. E. Hodson, O. I. Leszczyszyn, C. A. Blindauer, and S. R. Sturzenbaum. 2010. The two *Caenorhabditis elegans* metallothioneins (CeMT-1 and CeMT-2) discriminate between essential zinc and toxic cadmium. *FEBS J.* **277**: 2531–2542.
 53. Paton, C. M., and J. M. Ntambi. 2009. Biochemical and physiological function of stearoyl-CoA desaturase. *Am. J. Physiol. Endocrinol. Metab.* **297**: E28–E37.
 54. Brock, T. J., J. Browse, and J. L. Watts. 2007. Fatty acid desaturation and the regulation of adiposity in *Caenorhabditis elegans*. *Genetics*. **176**: 865–875.
 55. Perez, C. L., and M. R. Van Gilst. 2008. A ¹³C isotope labeling strategy reveals the influence of insulin signaling on lipogenesis in *C. elegans*. *Cell Metab.* **8**: 266–274.
 56. Gourley, B. L., S. B. Parker, B. J. Jones, K. B. Zumbrennen, and E. A. Leibold. 2003. Cytosolic aconitase and ferritin are regulated by iron in *Caenorhabditis elegans*. *J. Biol. Chem.* **278**: 3227–3234.
 57. Kim, Y. I., J. H. Cho, O. J. Yoo, and J. Ahn. 2004. Transcriptional regulation and life-span modulation of cytosolic aconitase and ferritin genes in *C. elegans*. *J. Mol. Biol.* **342**: 421–433.
 58. Wang, H., X. Jiang, J. Wu, L. Zhang, J. Huang, Y. Zhang, X. Zou, and B. Liang. 2016. Iron overload coordinately promotes ferritin expression and fat accumulation in *Caenorhabditis elegans*. *Genetics*. **203**: 241–253.
 59. Kashiwabara, Y., H. Nakagawa, G. Matsuki, and R. Sato. 1975. Effect of metal ions in the culture medium on the stearoyl-coenzyme a desaturase activity of *Mycobacterium phlei*. *J. Biochem.* **78**: 803–810.
 60. Romney, S. J., C. Thacker, and E. A. Leibold. 2008. An iron enhancer element in the FTN-1 gene directs iron-dependent expression in *Caenorhabditis elegans* intestine. *J. Biol. Chem.* **283**: 716–725.
 61. Behrouzian, B., and P. H. Buist. 2002. Fatty acid desaturation: variations on an oxidative theme. *Curr. Opin. Chem. Biol.* **6**: 577–582.
 62. Bai, Y., J. G. McCoy, E. J. Levin, P. Sobrado, K. R. Rajashankar, B. G. Fox, and M. Zhou. 2015. X-ray structure of a mammalian stearoyl-CoA desaturase. *Nature*. **524**: 252–256.
 63. Himoto, T., T. Nomura, J. Tani, H. Miyoshi, A. Morishita, H. Yoneyama, R. Haba, H. Masugata, and T. Masaki. 2015. Exacerbation of insulin resistance and hepatic steatosis deriving from zinc deficiency in patients with HCV-related chronic liver disease. *Biol. Trace Elem. Res.* **163**: 81–88.
 64. Bode, J. C., P. Hanisch, H. Henning, W. Koenig, F. W. Richter, and C. Bode. 1988. Hepatic zinc content in patients with various stages of alcoholic liver-disease and in patients with chronic active and chronic persistent hepatitis. *Hepatology*. **8**: 1605–1609.
 65. Ranasinghe, P., W. S. Wathurapatha, M. H. Ishara, R. Jayawardana, P. Galappathay, P. Katulanda, and G. R. Constantine. 2015. Effects of zinc supplementation on serum lipids: a systematic review and meta-analysis. *Nutr. Metab. (Lond)*. **12**: 26.
 66. Kang, X., W. Zhong, J. Liu, Z. Song, C. J. McClain, Y. J. Kang, and Z. Zhou. 2009. Zinc supplementation reverses alcohol-induced steatosis in mice through reactivating hepatocyte nuclear factor-4 alpha and peroxisome proliferator-activated receptor-alpha. *Hepatology*. **50**: 1241–1250.